Fault-Tolerant Control of Dual Three-Phase PMSM Drives With Minimized Copper Loss

Xueqing Wang, *Member, IEEE*, Zheng Wang, *Senior Member, IEEE*, Mingzhi He, *Member, IEEE*, Qun Zhou, *Member, IEEE*, Xueshan Liu, *Member, IEEE*, and Xin Meng, *Member, IEEE*

***Abstract*—In this article, a minimum-copper-loss fault-tolerant control scheme is proposed for open-phase fault and open-switch fault of dual three-phase permanent magnet synchronous motor (DT-PMSM) drives. Both the winding configurations of isolated neutral points and connected neutral points are studied in this article. In conventional minimum-copper-loss fault-tolerant control schemes, the constraints of sinusoidal phase currents result in insufficient copper-loss reduction. Different from them, the current references with the theoretically lowest copper losses are first derived and applied for different fault cases of DT-PMSM drives without using any unnecessary constraints in the proposed fault-tolerant control scheme. Thus, all phase currents in the proposed minimum-copper-loss fault-tolerant control scheme are optimized to be nonsinusoidal waveforms. Besides, the copper losses are further reduced by fully utilizing the remaining healthy switch in the faulty inverter leg for the open-switch fault of DT-PMSM drives with the proposed scheme. It has been theoretically and experimentally proved that the proposed fault-tolerant control scheme can reduce copper losses than all existing fault-tolerant schemes for both open-phase fault and open-switch fault in typical two-level voltage-source-inverter-fed DT-PMSM drives.**

***Index Terms*—Dual three-phase PMSM (DT-PMSM), fault-tolerant control, minimum loss, open-phase fault, open-switch fault.**

I. Introduction

With the increasing requirements in high power rating and high reliability of some modern industrial applications, such as aerospace, ship propulsion, and electric vehicle, the multiphase motor drives are experiencing fast development today [1]–[4]. The multiphase motor drives can usually continue to operate without stop when a fault occurs in the motor or inverter [5]. Among all the faults of motor drives, open-phase faults and open-switch faults are common and intensively studied [6]–[9].

For the open-phase fault of multiphase motor drive, the basic requirement of fault-tolerant control is eliminating the torque pulsations caused by the fault. The simplest solution is to remove the whole faulty winding to get smooth torque output [10], [11]. However, the maximum output power will be reduced greatly in this solution. For example, the maximum output power of dual three-phase permanent magnet synchronous motor (DT-PMSM) will be reduced by half after removing the faulty three-phase winding. Currently, most studies are dedicated to improving fault-tolerant performance by fully utilizing the healthy phases. In [12], the spatial distribution of voltage vectors is reconstructed based on the mathematical model of a five-phase induction motor with an open-phase fault. Then, a new lookup table composed of virtual voltage vectors is designed for direct torque control to tolerate the fault. In [13], model predictive torque control is combined with space vector modulation to improve both the dynamic response and steady-state control precision in the fault-tolerant operation of a five-phase PMSM with an open-phase fault. In [14], a decoupled model is proposed for five-phase PMSM with open-phase fault. Field-oriented control is combined with carrier-based pulsewidth modulation to tolerate the fault based on the concept of establishing equivalent rotating magnetomotive force. Literatures [15]–[17] take the reluctance torque of multiphase PMSMs under open-phase fault into consideration and proposed different maximum torque per ampere (MTPA)-based fault-tolerant control schemes to improve the torque output capability.

In the aspect of copper loss, the missing current in the faulty phase can only be compensated by increasing the current contributions of the remaining healthy phases in the fault-tolerant operation. Thus, the copper loss of a multiphase motor in the fault-tolerant operation will be larger than that in normal operation [18]. It should be noted that the copper loss usually dominates the total loss in electrical machines under high-load conditions. The increased copper loss may cause overheating if the fault-tolerant operation is sustained for a prolonged period of time [15]. Thus, reducing copper loss becomes very important in the fault-tolerant operation. In [19], different fault-tolerant current references are derived for the minimum-copper-loss operation of DT-PMSM drives with different winding configurations under open-phase fault conditions. Since only sinusoidal phase currents are considered, the copper loss can only be reduced to some extent. In [20] and [21], the copper loss of faulty

Manuscript received 18 November 2020; revised 1 March 2021; accepted 26 April 2021. Date of publication 29 April 2021; date of current version 30 July 2021. This work was supported in part by the Natural Science Foundation of China under Grant 52077034 and in part by the Fundamental Research Funds for the Central Universities under Grant YJ202080. Recommended for publication by Associate Editor T. Shi. *(Corresponding author: Mingzhi He.)*

Xueqing Wang, Mingzhi He, Qun Zhou, Xueshan Liu, and Xin Meng are with the College of Electrical Engineering, Sichuan University, Chengdu 610065, China (e-mail: xwang@scu.edu.cn; darmyhe@vip.126.com; zhouqunsc@163.com; xueshan5851@163.com; mengxin_pe@163.com).

Zheng Wang is with the School of Electrical Engineering, Southeast University, Nanjing 210096, China (e-mail: zwang@eee.hku.hk).

Color versions of one or more figures in this article are available at https://doi.org/10.1109/TPEL.2021.3076509.

Color versions of one or more figures in this article are available at https://doi.org/10.1109/TPEL.2021.3076509.

Digital Object Identifier 10.1109/TPEL.2021.3076509

DT-PMSM with isolated neutral points is further reduced by minimizing the *d*-axis current of the healthy three-phase winding to zero. Due to the adoption of sinusoidal phase currents in the faulty three-phase winding, the copper loss in this solution is still optimized incompletely. The minimum-copper-loss solution for the open-phase fault of DT-PMSM still needs to be further investigated.

As for the open-switch fault in multiphase motor drive, the whole faulty inverter leg comprising the faulty switch is usually removed, and then, the open-switch fault will be tolerated in the same way as fault-tolerant control for open-phase fault [22], [23]. On the other hand, some auxiliary circuits and high-reliability inverter topologies have been developed to cope with the open-switch faults. The solutions of various auxiliary circuits are usually fulfilled by connecting neutral points of motor stator windings or connecting the winding terminal of the faulty phase to a voltage source, which can be the midpoint of the dc-link or a redundant inverter leg [23], [24]. In the aspect of high-reliability inverter topologies, the basic fault-tolerant idea is using the remaining voltage vectors of the inverters after fault to generate required voltages. The candidate high-reliability inverter topologies can be multilevel inverters or matrix inverters [25]–[28]. Although the solutions using auxiliary circuits and high-reliability inverter topologies can improve the fault-tolerant performances, the costs will be increased inevitably due to additional hardware of power inverters. Thus, it is meaningful to improve the fault-tolerant capability of multiphase motor drives by fully utilizing the remaining healthy switches in the faulty inverter leg without any auxiliary circuits.

Based on the existing research foundation and shortcomings mentioned earlier, this article aims at exploring the limit of the copper loss reduction in the fault-tolerant operation of typical two-level voltage source inverter (VSI)-fed DT-PMSM drives. First, the fault-tolerant current references with the theoretically lowest copper losses are derived for the open-phase fault of DT-PMSM drives with isolated neutral points and connected neutral points without using any unnecessary constraints. Second, a two-mode minimum-copper-loss fault-tolerant control scheme is proposed for the open-switch fault of DT-PMSM drives with isolated neutral points and connected neutral points by fully utilizing the remaining healthy switch in the faulty inverter leg. Third, the proposed minimum-copper-loss fault-tolerant control scheme is compared with three existing typical minimum-copper-loss fault-tolerant control schemes to show its superiority in copper loss reduction. In this article, only the single open-phase fault and single open-switch fault of DT-PMSM drives are studied. The proposed minimum-copper-loss fault-tolerant control scheme is only suitable for the surface-mounted DT-PMSM drives.

The rest content of this article is organized as follows. The mathematical model and control framework of DT-PMSM are presented in Section II. Then, the fault-tolerant control is studied comprehensively to minimize the copper loss for the open-phase fault of DT-PMSM drives with different winding configurations in Section III. In Section IV, a two-mode minimum-copper-loss fault-tolerant control scheme is proposed for the open-switch fault by fully utilizing the remaining healthy switch in the faulty inverter leg. In Section V, the proposed fault-tolerant control scheme is compared with the existing fault-tolerant control schemes to prove its superiority. In Section VI, experimental results are presented to verify the effectiveness of the proposed schemes. Finally, Section VII concludes this article.

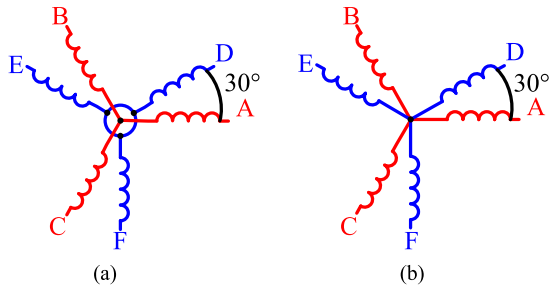

Fig. 1. Winding configurations of DT-PMSM. (a) Isolated neutral points. (b) Connected neutral points.

II. Modeling and Control

A. Modeling of DT-PMSM

The DT-PMSM has two sets of three-phase windings, which are spatially shifted by 30 electric degrees. The common winding configurations of DT-PMSM include isolated neutral points and connected neutral points, as shown in Fig. 1. The main difference is that the zero-sequence current path is blocked in the DT-PMSM with isolated neutral points but unobstructed in the DT-PMSM with connected neutral points. Thus, the DT-PMSM with isolated neutral points has the merits of low control complexity due to its low control dimension, whereas the DT-PMSM with connected neutral points has the advantages of better fault-tolerant capability due to its high control dimension. In general, the two winding configurations of the DT-PMSM have their respective advantages and they are usually determined according to the practical applications. In this article, both the two winding configurations of the DT-PMSM will be discussed.

The DT-PMSM is a nonlinear high-order system, which makes analysis and control difficult. By using the vector space decomposition (VSD) method, the voltage and current space vectors of the DT-PMSM can be decoupled into three two-dimensional orthogonal subspaces: α–β (torque subspace), x–y (harmonic subspace), and o_1–o_2 [29]. Following equation shows the decomposition matrix of the VSD method for DT-PMSM:

$$[\mathbf{T}_{\mathrm{VSD}}] = \begin{bmatrix} \alpha \\ \beta \\ x \\ y \\ o_1 \\ o_2 \end{bmatrix} = \frac{1}{6} \begin{bmatrix} 2 & -1 & -1 & \sqrt{3} & -\sqrt{3} & 0 \\ 0 & \sqrt{3} & -\sqrt{3} & 1 & 1 & -2 \\ 2 & -1 & -1 & -\sqrt{3} & \sqrt{3} & 0 \\ 0 & -\sqrt{3} & \sqrt{3} & 1 & 1 & -2 \\ 2 & 2 & 2 & 0 & 0 & 0 \\ 0 & 0 & 0 & 2 & 2 & 2 \end{bmatrix}. \quad (1)$$

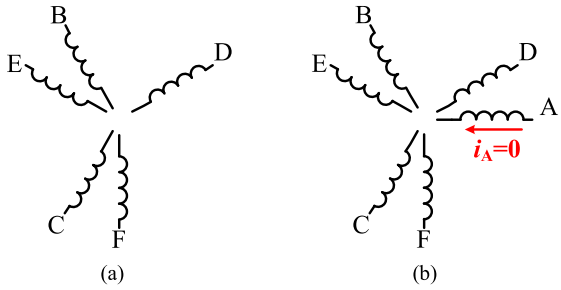

Fig. 2. Conversions of open-phase fault in DT-PMSM. (a) Abnormal five-phase PMSM. (b) Virtual dual-three-phase PMSM.

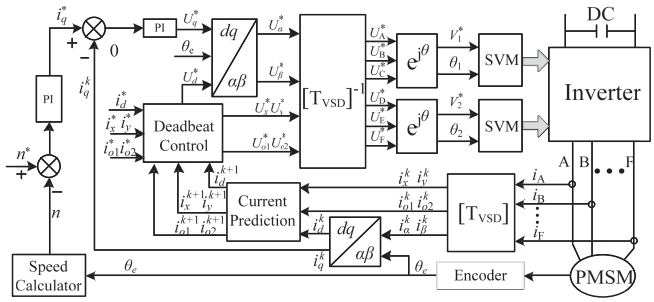

Fig. 3. Control block diagram of DT-PMSM.

In this way, the voltage and torque equations of DT-PMSM can be obtained, as shown in the following equation:

$$\begin{cases} u_d = R_s i_d + L_d di_d/dt - \omega_r L_q i_q \\ u_q = R_s i_q + L_q di_q/dt + \omega_r L_d i_d + \omega_r \psi_f \\ u_x = R_s i_x + L_{ls} di_x/dt \\ u_y = R_s i_y + L_{ls} di_y/dt \\ u_{o1} = R_s i_{o1} + L_{ls} di_{o1}/dt \\ u_{o2} = R_s i_{o2} + L_{ls} di_{o2}/dt \end{cases} \tag{2}$$

$$T_e = 3n_p \left(\psi_f i_q + (L_d - L_q) i_d i_q\right) \tag{3}$$

where R_s is the stator resistance. L_d, L_q, and L_{ls} are the d-axis inductance, the q-axis inductance, and the stator leakage inductance, respectively. ω_r is the rotor angular velocity and ψ_f is the amplitude of rotor flux. n_p is pole pair number.

B. Control Framework

In the conventional fault-tolerant schemes for dual three-phase motor, the faulty motor is usually considered as an abnormal five-phase machine, as shown in Fig. 2(a) and the machine model will be reconstructed according to the spatial distribution of the remaining healthy phase windings [12], [31]. As a result, both the decoupling matrix and the space vector diagram have to be redesigned. Different from them, a concept of virtual healthy machine is adopted when designing the uniform control framework of DT-PMSM for both normal and fault-tolerant operations, as shown in Fig. 2(b). The additional constraint of the fault-tolerant control for the virtual dual DT-PMSM is that the current reference of the faulty phase should be zero. Based on the constraint, several rules should be satisfied when designing the uniform control framework, namely closed-loop control on all subspaces, separate modulation between two three-phase inverters, and dc and non-dc current tracking capability of the closed-loop control on d-axis, x–y subspace, and o_1–o_2 subspace. According to the design rules, a uniform control framework for both normal and fault-tolerant operations is designed, as shown in Fig. 3. When the control mode change from normal operation to fault-tolerant operation, the fault-tolerant control can be fulfilled by simply replacing the current references of zero on d-axis, x–y subspace, and o_1–o_2 subspace with the proposed current references in this article without changing the machine model, modulation strategy, and the control structure.

In Fig. 3, the typical PI control is adopted in the q-axis for the precise closed-loop control for the torque. For d-axis, x–y subspace, and o_1–o_2 subspace, the deadbeat predictive current control in [30] is adopted to achieve effective tracking for both the dc and non-dc current references under normal and fault-tolerant operations. It should be noted that the currents on o_1–o_2 subspace remain zeros for the DT-PMSM with isolated neutral points and the closed-loop control of currents on o_1–o_2 subspace can be ignored. In Fig. 3, the VSD transformation and its inverse transformation are adopted to achieve the decoupling control of α–β, x–y, and o_1–o_2 subspace. Two identical three-phase SVMs are utilized to simplify the modulation process.

III. Minimum-Copper-Loss Fault-Tolerant Control Scheme for Open-Phase Fault

A. Correlations of the Currents on Different Coordinates

The decoupled coordinate systems from VSD transformation, namely α–β subspace, x–y subspace, and o_1–o_2 subspaces, are usually adopted in different control methods to improve the control performances of DT-PMSM. It is inappropriate to use them to analyze the faults, due to the complex coupling relations between the decoupled coordinate systems and the faulty phase. To simplify the fault analysis and the solution of fault-tolerant current references with minimum copper loss, two rotating coordinate systems, namely d_1–q_1 and d_2–q_2, are introduced, which are established based on phase-ABC and phase-DEF, respectively. According to the Park transformation, the currents on d_1–q_1 and d_2–q_2 coordinate systems can be calculated as expressed in (4) shown at the bottom of the next page. It can be observed from (4) that the currents on d_1–q_1 and d_2–q_2 coordinate systems are separately related to the phase-ABC currents and phase-DEF currents. In this way, the constraint equation of the current in the faulty phase can be greatly simplified by reducing the number of current variables. By using the inverse transformation of (4), the phase currents can be expressed with the currents on d_1–q_1 and d_2–q_2 coordinate systems, as shown in (5) shown at the bottom of the next page. Then, the constraint equation of the current in the faulty phase can be directly constructed according to (5). This constraint equation is completely determined by the electrical characteristics of the faulty motor drive and remains unchanged after the open-phase fault.

To achieve the minimum copper loss under fault-tolerant operation, the copper loss equation of DT-PMSM should be established as the necessary foundation of current optimization. The theoretical average copper loss of DT-PMSM can be directly calculated by summing over the copper losses of the six stator windings, as expressed in

$$\overline{P_{\mathrm{Cu}}} = \frac{1}{2\pi}\int_0^{2\pi} \left(i_{\mathrm{A}}^2 + i_{\mathrm{B}}^2 + i_{\mathrm{C}}^2 + i_{\mathrm{D}}^2 + i_{\mathrm{E}}^2 + i_{\mathrm{F}}^2\right) R_s d\theta_e. \quad (6)$$

By substituting (5) into (6), the copper loss of DT-PMSM can be expressed with the currents in d_1–q_1 and d_2–q_2 coordinate systems, as shown in (7). In this way, the average copper loss of DT-PMSM in the fault-tolerant operation can be minimized by optimizing the currents in d_1–q_1 and d_2–q_2 coordinate systems

$$\overline{P_{\mathrm{Cu}}} = \frac{1}{2\pi}\int_0^{2\pi} \frac{3}{2}\left(i_{d1}^2 + i_{q1}^2 + i_{d2}^2 + i_{q2}^2 + 2i_{o1}^2 + 2i_{o2}^2\right) R_s d\theta_e. \quad (7)$$

B. Configuration of Isolated Neutral Points

When an open-phase fault occurs in the DT-PMSM drive, the current of the faulty phase winding will be forced to be zero. Taking Phase-A open-phase fault as an example, the Phase-A current i_{A} will become zero after fault, which is the basic and necessary constraint in the process of optimizing the minimum-copper-loss fault-tolerant current references. For the DT-PMSM with isolated neutral points, the zero-sequence current path is blocked. Thus, the zero-sequence currents i_{o1} and i_{o2} are both zero and no current optimization is required for the corresponding current references i_{o1}^* and i_{o2}^*. By setting the current i_{A}, i_{o1}, and i_{o2} in (5) to zero, the constraint of current references in d_1–q_1 coordinate system can be obtained from (5) as

$$i_{d1}^* \cos(\theta_e) - i_{q1}^* \sin(\theta_e) = 0. \quad (8)$$

Another basic constraint for the fault-tolerant control of DT-PMSM is that the sum of the torque contributions from two three-phase windings should meet the requirement of the general torque output. In other words, the sum of the current reference from two three-phase windings should meet the requirement of the general current references. Since the equal amplitude transformation is adopted as the rule of all transformations in this article, the sum of the current references i_{q1}^* and i_{q2}^* should be equal to $2i_q^*$ in the fault-tolerant operation, as expressed in

$$i_{q1}^* + i_{q2}^* = 2i_q^*. \quad (9)$$

For the open-phase fault of DT-PMSM with isolated neutral points, only the two constraints above can be adopted as the basic constraints of the minimum-copper-loss fault-tolerant control. The other constraints should all be used to fully optimize the copper loss. Otherwise, the copper loss can hardly be minimized. It can be observed that the d_2-axis current reference i_{d2}^* has no coupling with (8) and (9). Thus, the optimal value of $i_{d2}*$ should remain zero to minimize the loss production from the d_2-axis current. It is known that the minimum copper loss of motor drive can be achieved by minimizing the instantaneous copper loss. By combining (8) and (9) with (7), the instantaneous copper loss of DT-PMSM with isolated neutral points can be expressed as

$$P_{\mathrm{Cu}} = \frac{3}{2}\left((2+\tan^2(\theta_e))i_{q1}^{*2} - 4i_q^* i_{q1}^* + 4i_q^{*2}\right) R_s. \quad (10)$$

According to (10), the instantaneous copper loss P_{Cu} is a quadratic equation and the second-order coefficient of the q_1-axis current reference i_{q1}^* is constantly positive. Thus, the instantaneous copper loss P_{Cu} has a unique minimum point in arbitrary angle. Therefore, the minimum-copper-loss constraint can be established by using the derivative of the instantaneous copper loss P_{Cu}, as expressed in

$$\frac{d\left((2+\tan^2(\theta_e))i_{q1}^{*2} - 4i_q^* i_{q1}^* + 4i_q^{*2}\right)}{d(i_{q1}^*)} = 0. \quad (11)$$

By combining (8), (9), and (11), the minimum-copper-loss current references in d_1–q_1 and d_2–q_2 coordinate systems can

$$\begin{bmatrix} i_{d1} \\ i_{q1} \\ i_{o1} \\ i_{d2} \\ i_{q2} \\ i_{o2} \end{bmatrix} = \frac{2}{3}\begin{bmatrix} \cos(\theta_e) & \cos\left(\theta_e - \frac{2}{3}\pi\right) & \cos\left(\theta_e + \frac{2}{3}\pi\right) & 0 & 0 & 0 \\ \sin(\theta_e+\pi) & \sin\left(\theta_e + \frac{1}{3}\pi\right) & \sin\left(\theta_e - \frac{1}{3}\pi\right) & 0 & 0 & 0 \\ \frac{1}{2} & \frac{1}{2} & \frac{1}{2} & 0 & 0 & 0 \\ 0 & 0 & 0 & \cos\left(\theta_e - \frac{1}{6}\pi\right) & \cos\left(\theta_e - \frac{5}{6}\pi\right) & \cos\left(\theta_e + \frac{1}{2}\pi\right) \\ 0 & 0 & 0 & \sin\left(\theta_e + \frac{5}{6}\pi\right) & \sin\left(\theta_e + \frac{1}{6}\pi\right) & \sin(\theta_e - \frac{1}{2}\pi) \\ 0 & 0 & 0 & \frac{1}{2} & \frac{1}{2} & \frac{1}{2} \end{bmatrix} \begin{bmatrix} i_{\mathrm{A}} \\ i_{\mathrm{B}} \\ i_{\mathrm{C}} \\ i_{\mathrm{D}} \\ i_{\mathrm{E}} \\ i_{\mathrm{F}} \end{bmatrix} \quad (4)$$

$$\begin{bmatrix} i_{\mathrm{A}} \\ i_{\mathrm{B}} \\ i_{\mathrm{C}} \\ i_{\mathrm{D}} \\ i_{\mathrm{E}} \\ i_{\mathrm{F}} \end{bmatrix} = \begin{bmatrix} \cos(\theta_e) & -\sin(\theta_e) & 1 & 0 & 0 & 0 \\ \cos(\theta_e - \frac{2}{3}\pi) & -\sin(\theta_e - \frac{2}{3}\pi) & 1 & 0 & 0 & 0 \\ \cos(\theta_e + \frac{2}{3}\pi) & -\sin(\theta_e + \frac{2}{3}\pi) & 1 & 0 & 0 & 0 \\ 0 & 0 & 0 & \cos(\theta_e - \frac{1}{6}\pi) & -\sin(\theta_e - \frac{1}{6}\pi) & 1 \\ 0 & 0 & 0 & \cos(\theta_e - \frac{5}{6}\pi) & -\sin(\theta_e - \frac{5}{6}\pi) & 1 \\ 0 & 0 & 0 & \cos(\theta_e + \frac{1}{2}\pi) & -\sin(\theta_e + \frac{1}{2}\pi) & 1 \end{bmatrix} \begin{bmatrix} i_{d1} \\ i_{q1} \\ i_{o1} \\ i_{d2} \\ i_{q2} \\ i_{o2} \end{bmatrix} \quad (5)$$

be solved as

$$\begin{cases} i_{d1}^* = \frac{2\sin(2\theta_e)}{3+\cos(2\theta_e)} i_q^* \\ i_{q1}^* = \frac{2+2\cos(2\theta_e)}{3+\cos(2\theta_e)} i_q^* \\ i_{o1}^* = 0 \\ i_{d2}^* = 0 \\ i_{q2}^* = \frac{4}{3+\cos(2\theta_e)} i_q^* \\ i_{o2}^* = 0. \end{cases} \tag{12}$$

It should be noted that the minimum-copper-loss current references apply equally to the faults in other phases. Only minor adjustments are required. It can be observed from Fig. 1 that the six-phase windings are symmetrically distributed in space. The phase shifts between Phase-A and other phases (Phase-B, Phase-C, Phase-D, Phase-E, and Phase-F) are $2\pi/3$, $4\pi/3$, $\pi/6$, $5\pi/6$, and $3\pi/2$, respectively. Thus, minimum-copper-loss current references in d_1–q_1 and d_2–q_2 coordinate systems under Phase-B fault and Phase-C fault can be obtained by replacing θ_e in (12) with θ_e–$2\pi/3$ and θ_e–$4\pi/3$, respectively. Since the Phase-ABC currents and Phase-DEF currents are transformed into two different coordinate systems, the acquirement of minimum-copper-loss current references in d_1–q_1 and d_2–q_2 coordinate systems under the faults of Phase-D, Phase-E, and Phase-F should swap the current references in different coordinate systems of (12) and replacing θ_e with θ_e–$\pi/6$, θ_e–$5\pi/6$, and θ_e–$3\pi/2$, respectively. In this way, the minimum-copper-loss current references under the faults of different phases can be obtained. For example, the minimum-copper-loss current references in d_1–q_1 and d_2–q_2 coordinate systems under Phase-D open-phase fault can be expressed as

$$\begin{cases} i_{d1}^* = 0 \\ i_{q1}^* = \frac{4}{3+\cos(2\theta_e-\pi/3)} i_q^* \\ i_{o1}^* = 0 \\ i_{d2}^* = \frac{2\sin(2\theta_e-\pi/3)}{3+\cos(2\theta_e-\pi/3)} i_q^* \\ i_{q2}^* = \frac{2+2\cos(2\theta_e-\pi/3)}{3+\cos(2\theta_e-\pi/3)} i_q^* \\ i_{o2}^* = 0. \end{cases} \tag{13}$$

Considering that decoupled coordinate systems from VSD transformation have obvious superiority in the aspect of fault-tolerant control of DT-PMSM drive, the minimum-copper-loss current references in d_1–q_1 and d_2–q_2 coordinate systems should be transformed into α–β, x–y, and o_1–o_2 subspaces for closed-loop current control. By combining (2), (5), and the rotating transformation in (14), the currents on α–β, x–y, and o_1–o_2 subspaces can be expressed with the currents in d_1–q_1 and d_2–q_2 coordinate systems, as shown in (15)

$$\begin{bmatrix} i_d \\ i_q \end{bmatrix} = \begin{bmatrix} \cos(\theta_e) & \sin(\theta_e) \\ -\sin(\theta_e) & \cos(\theta_e) \end{bmatrix} \begin{bmatrix} i_\alpha \\ i_\beta \end{bmatrix} \tag{14}$$

$$\begin{bmatrix} i_d \\ i_q \\ i_x \\ i_y \\ i_{o1} \\ i_{o2} \end{bmatrix} = \frac{1}{2} \begin{bmatrix} 1 & 0 & 0 & 1 & 0 & 0 \\ 0 & 1 & 0 & 0 & 1 & 0 \\ \cos(\theta_e) & -\sin(\theta_e) & 0 & -\cos(\theta_e) & \sin(\theta_e) & 0 \\ -\sin(\theta_e) & -\cos(\theta_e) & 0 & \sin(\theta_e) & \cos(\theta_e) & 0 \\ 0 & 0 & 2 & 0 & 0 & 0 \\ 0 & 0 & 0 & 0 & 0 & 2 \end{bmatrix} \begin{bmatrix} i_{d1} \\ i_{q1} \\ i_{o1} \\ i_{d2} \\ i_{q2} \\ i_{o2} \end{bmatrix}. \tag{15}$$

Then, the minimum-copper-loss current references on α–β, x–y, and o_1–o_2 subspaces can be expressed with the q-axis current reference i_q^* by substituting (11) into (15), as shown in (16). The q-axis current reference $i_q{}^*$ can be obtained from the speed PI controller in Fig. 2. Finally, the minimum-copper-loss fault-tolerant control for the open-phase fault of DT-PMSM drive with isolated neutral points can be fulfilled by using the current references from the following equation in the control diagram in Fig. 2:

$$\begin{cases} i_d^* = \frac{\sin(2\theta_e)}{3+\cos(2\theta_e)} i_q^* \\ i_x^* = \frac{2\sin(\theta_e)}{3+\cos(2\theta_e)} i_q^* \\ i_y^* = 0 \\ i_{o1}^* = 0 \\ i_{o2}^* = 0. \end{cases} \tag{16}$$

With (16), the waveforms of the minimum-copper-loss current references on α–β, x–y, and o_1–o_2 subspaces for the Phase-A open-phase fault of DT-PMSM drive with isolated neutral points can be plotted, as shown in Fig. 4(a). For ease of understanding, the currents in Fig. 4 are expressed in the form of per unit (p.u.) relative to the q-axis current reference. By transforming the current references from the decoupled coordinate systems into the six-phase stationary coordinate system, the six-phase current references can be plotted, as shown in Fig. 4(b). The zero Phase-A current reference in Fig. 4(b) proves the correctness of the theoretical analysis and the deduced current references in (16). In the same way, the waveforms of the minimum-copper-loss current references for the Phase-D open-phase fault can be plotted, as shown in Fig. 5. It can be found that the copper losses with the proposed fault-tolerant control for different open-phase faults are identical.

C. Configuration of Connected Neutral Points

Different from the DT-PMSM with isolated neutral points, the DT-PMSM with connected neutral points can provide a zero-sequence current path. Thus, the dimension of current control will increase and the copper loss can be further reduced. Due to the existence of the zero-sequence current path in the DT-PMSM with connected neutral points, the zero-sequence currents i_{o1} and i_{o2} can be optimized to reduce copper loss.

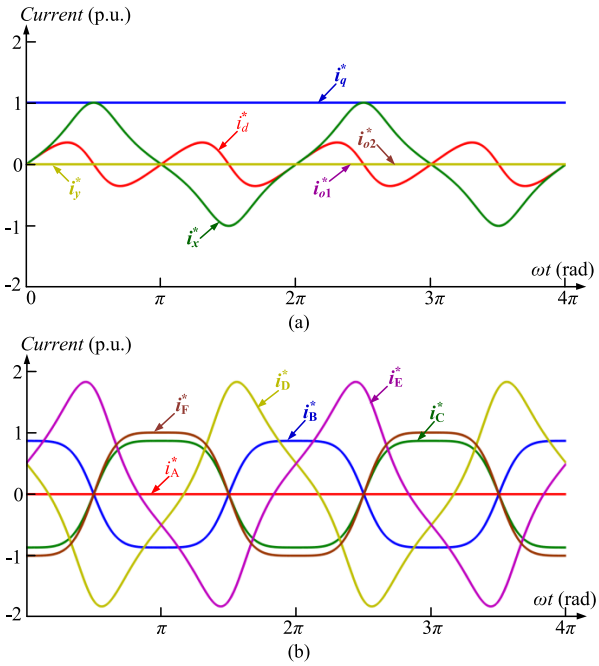

Fig. 4. Current references of the proposed minimum-copper-loss fault-tolerant control for Phase-A open-phase fault of DT-PMSM drive with isolated neutral points. (a) Currents on α–β, x–y, and o_1–o_2 subspaces. (b) Phase currents.

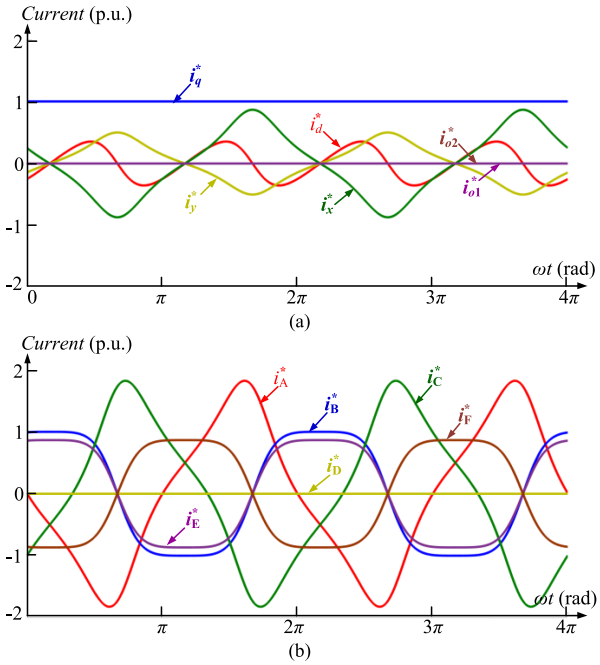

Fig. 5. Current references of the proposed minimum-copper-loss fault-tolerant control for Phase-D open-phase fault of DT-PMSM drive with isolated neutral points. (a) Currents on α–β, x–y, and o_1–o_2 subspaces. (b) Phase currents.

By setting the current i_{A} in (5) to zero, the constraint of current references in d_1–q_1 coordinate system can be expressed as the first equation in (17). Same as the case of isolated neutral points, the sum of the current references i_{q1}^* and i_{q2}^* should also be equal to $2iq^*$ in the fault-tolerant operation, as expressed in the second equation of (17). Besides, since only one current path exists between two three-phase windings, the sum of two zero-sequence current references i_{o1}^* and i_{o2}^* should be zero. For the open-phase fault of DT-PMSM with connected neutral points, only the three constraints above can be adopted as the basic constraints of the minimum-copper-loss fault-tolerant control. The other constraints should all be used to fully optimize the copper loss

$$\begin{cases} i_{d1}^*\cos(\theta_e) - i_{q1}^*\sin(\theta_e) + i_{o1}^* = 0 \\ i_{q1}^* + i_{q2}^* = 2i_q^* \\ i_{o1}^* + i_{o2}^* = 0 \\ \frac{\partial(i_{d1}^{*\,2}+i_{q1}^{*\,2}+i_{d2}^{*\,2}+i_{q2}^{*\,2}+2i_{o1}^{*\,2}+2i_{o2}^{*\,2})}{\partial i_{d1}^*} = 0 \\ \frac{\partial(i_{d1}^{*\,2}+i_{q1}^{*\,2}+i_{d2}^{*\,2}+i_{q2}^{*\,2}+2i_{o1}^{*\,2}+2i_{o2}^{*\,2})}{\partial i_{q1}^*} = 0. \end{cases} \tag{17}$$

According to (7), minimum copper loss of DT-PMSM with connected neutral points can be achieved by minimizing the instantaneous sum of the squares of the currents i_{d1}, i_{q1}, i_{o1}, i_{d2}, i_{q2}, and i_{o2}. Due to the increase in the number of variables, two minimum-copper-loss constraints are required to fully optimize the current references. Based on this analysis, two minimum-copper-loss constraints are established by using the partial derivatives of the instantaneous sum, as expressed in (17). It can be observed from (17) that the d_2-axis current reference i_{d2}^* has no coupling with the first three equations. Thus, the optimal value of i_{d2}^* should remain zero to minimize the loss production from d_2-axis current, according to (7). By combining all equations in (17), the minimum-copper-loss current references in d_1–q_1 and d_2–q_2 coordinate systems can be solved as

$$\begin{cases} i_{d1}^* = \frac{2\sin(2\theta_e)}{4+\cos(2\theta_e)} i_q^* \\ i_{q1}^* = \frac{3+2\cos(2\theta_e)}{4+\cos(2\theta_e)} i_q^* \\ i_{o1}^* = \frac{\sin(\theta_e)}{4+\cos(2\theta_e)} i_q^* \\ i_{d2}^* = 0 \\ i_{q2}^* = \frac{5}{4+\cos(2\theta_e)} i_q^* \\ i_{o2}^* = -\frac{\sin(\theta_e)}{4+\cos(2\theta_e)} i_q^*. \end{cases} \tag{18}$$

Then, the minimum-copper-loss current references on α–β, x–y, and o_1–o_2 subspaces can be expressed with the q-axis current reference $i_q{}^*$ by substituting (18) into (14), as shown in (19). Finally, the proposed minimum-copper-loss fault-tolerant control for the open-phase fault of DT-PMSM drive with connected neutral points can be fulfilled by using the current references from (19) in the control diagram in Fig. 2.

According to (19), the waveforms of the minimum-copper-loss current references on α–β, x–y, and o_1–o_2 subspaces for the open-phase fault of DT-PMSM drive with connected neutral points can be plotted, as shown in Fig. 6(a). By comparing the current waveforms in Figs. 4(a) and 6(a), it can be observed that the x-axis current references $i_x{}^*$ can be reduced greatly by using the zero-sequence current path. Thus, the positive role of the zero-sequence current path in copper loss reduction can be presented more intuitively. By transforming the current references from the decoupled coordinate systems into the six-phase stationary coordinate system, the six-phase current references can be plotted, as shown in Fig. 6(b). The zero Phase-A current reference in Fig. 6(b) proves the correctness of the theoretical

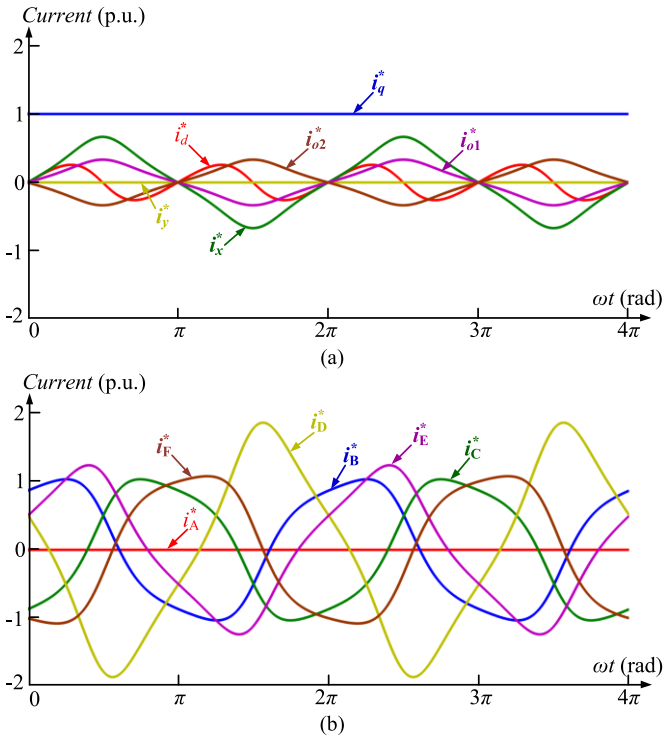

Fig. 6. Current references of the proposed minimum-copper-loss fault-tolerant control for Phase-A open-phase fault of DT-PMSM drive with connected neutral points. (a) Currents on α–β, x–y, and o_1–o_2 subspaces. (b) Phase currents.

analysis and the deduced current references in

$$\begin{cases} i_d^* = \frac{\sin(2\theta_e)}{4+\cos(2\theta_e)} i_q^* \\ i_x^* = \frac{2\sin(\theta_e)}{4+\cos(2\theta_e)} i_q^* \\ i_y^* = 0 \\ i_{o1}^* = \frac{\sin(\theta_e)}{4+\cos(2\theta_e)} i_q^* \\ i_{o2}^* = -\frac{\sin(\theta_e)}{4+\cos(2\theta_e)} i_q^*. \end{cases} \tag{19}$$

To acquire the spectrum characteristics of the current references in the proposed fault-tolerant control scheme, the FFT analysis of the non-dc current references in Fig. 6(a) has been conducted, as shown in Fig. 7. The q-axis current reference is adopted as the base value. It can be found from Fig. 7(a) that the d-axis current contains second and fourth harmonic components. In Fig. 7(b), the fundamental current dominates the x-axis current reference, which contains few third and fifth harmonic components. For the o_1-axis current reference in Fig. 7(c), fundamental and third harmonic components are included. It can be concluded that the main orders of current references are all no more than 5. Due to the low-frequency characteristics of the current references and the relatively high control bandwidth of the deadbeat control with 5-kHz sampling frequency, the uniform control framework in Fig. 3 can guarantee effective fault-tolerant control. The deadbeat controller in Fig. 3 can also be replaced with other high-performance controllers possessing the dc and non-dc current tracking capability to achieve better control performance.

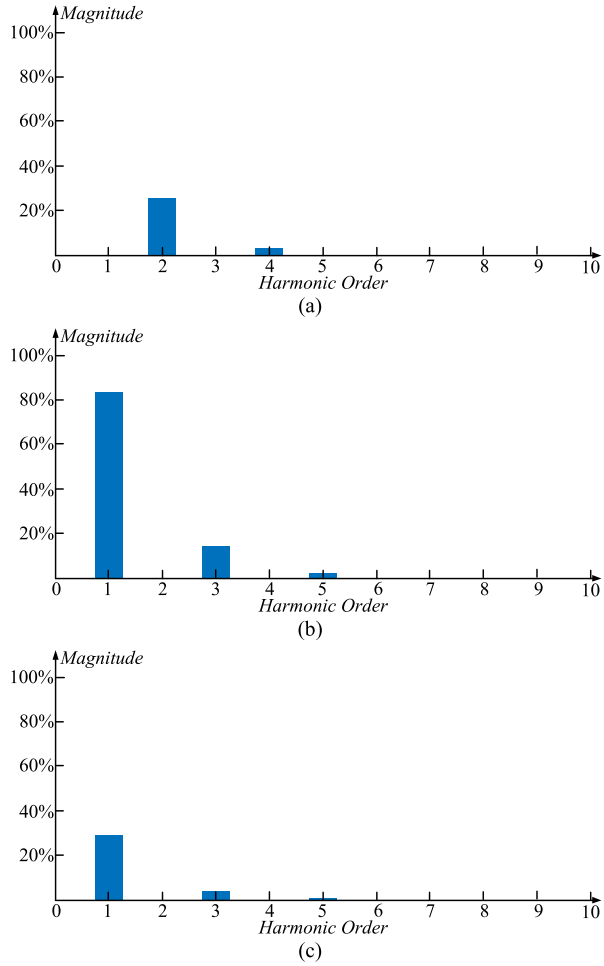

Fig. 7. FFT analysis of current references in the proposed fault-tolerant control scheme for Phase-A open-phase fault of DT-PMSM drive with connected neutral points. (a) d-axis current. (b) x-axis current. (c) o_1-axis current.

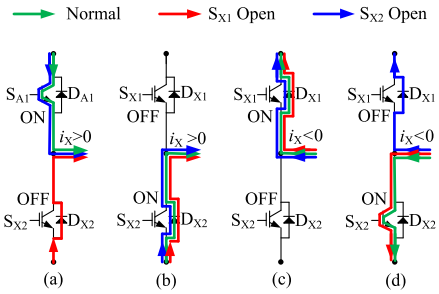

Fig. 8. Current paths under different operation states. (a) $i_X>0$: S_{X1} ON, S_{X2} OFF. (b) $i_X>0$: S_{X1} OFF, S_{X2} ON. (c) $i_X<0$: S_{X1} ON, S_{X2} OFF. (d) $i_X<0$: S_{X1} OFF, S_{X2} ON.

IV. Minimum-Copper-Loss Fault-Tolerant Control Scheme for Open-Switch Fault

A. Operation Analysis of Faulty Inverter Leg

To clarify the impacts of open-switch faults on the operation of faulty inverter leg, Fig. 8 shows the current paths in faulty inverter leg under different switching states and current directions. Since the operation principles of all phase legs are identical, the subscript X is used in Fig. 8 to refer to Phase-X. By combining

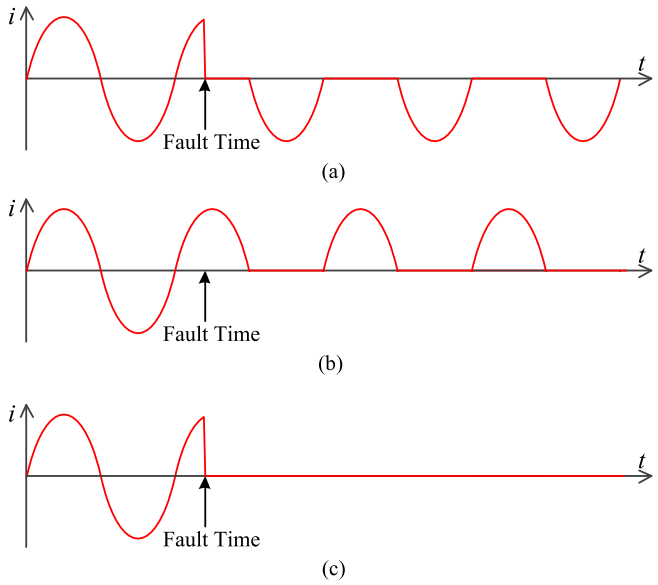

Fig. 9. Faulty phase current under different faults. (a) S_{X1} open-switch fault. (b) S_{X2} open-switch fault. (c) Open-phase fault.

different current directions with different switching states, four different operation states can be obtained in Fig. 8(a)–(d). The two-level inverter can generate two voltage levels, namely U_{DC} (Level-P) and 0 (Level-N). In Fig. 8, the current paths under normal operation are marked with green. The red and blue paths represent the current routes under open-switch faults in upper switch S_{X1} and lower S_{X2}, respectively. Under normal operation, the level-P is output by turning ON the upper switch S_{X1} and the level-N is generated by turning ON lower switch S_{X2}. The switching states of S_{X1} and S_{X2} are complementary with each other to avoid the short-circuit fault of dc-bus. When the phase-X current flows out of the inverter leg, namely $i_X>0$, the current goes through the upper switch S_{X1} under the state of Level-P, and goes through the lower diode D_{X2} under the state of Level-N, as shown in Fig. 8(a) and (b). Equally, when the phase-X current flows into the inverter leg, namely $i_X<0$, the current goes through the upper diode D_{X1} under the state of Level-P, and goes through the lower switch S_{X2} under the state of Level-N, as shown in Fig. 8(c) and (d), respectively. Since the current paths in Fig. 8 are constructed according to the inherent characteristics of the full-bridge inverter mentioned earlier, they are applicable to any mode of four-quadrant operation, including the regenerative mode.

When an open-switch fault occurs in S_{X1}, the current flowing through the switch S_{X1} will be blocked, and the level-P will be changed to be the level-N in the state of Phase-X current outflow in Fig. 8(a). The other operation states are not affected in Fig. 8(b)–(d). As a result, the level-N from the faulty Phase-X inverter leg will force the positive Phase-X current to decrease until zero. Because of the absence of current path, the faulty phase will operate under temporary open-circuit state and the current in the faulty phase will remain zero until the faulty phase enters the negative half fundamental period, as shown in Fig. 9(a). Therefore, the phase current returns to normal in every negative half fundamental period of the faulty phase. When S_{X2} is with the open-switch fault, the current flowing through the switch S_{X2} will be blocked, and the level-N will be changed to the level-P in the state of Phase-X current inflow, as shown in Fig. 8(d). As a result, the level-P from the faulty Phase-X inverter leg will force the negative Phase-X current to increase until zero. The other operation states can still output the voltage levels normally, as shown in Fig. 8(a)–(c). Equally, the current in the faulty phase will remain zero until the faulty phase enters the positive half fundamental period, as shown in Fig. 9(b). Since S_{X2} open-switch fault happens in the positive half fundamental period in Fig. 9(b), the fault feature will occur in the coming negative half fundamental period. By comparison, the open-phase fault will force the current in the faulty phase to be consistent zero, as shown in Fig. 9(c). To achieve better fault-tolerant performance, different current references will be proposed for the different faults in the same faulty phase. It can be found from Fig. 9 that it is easy to identify different faults in the same faulty phase by observing the average current of the faulty phase [32]. Compared with conventional fault-tolerant solutions, the proposed scheme can achieve lower copper losses under different faults without increasing too much burden for the fault diagnosis. Besides, distinguishing different faults in the same faulty phase during the fault diagnosis process is helpful for later maintenance. Therefore, it is worth identifying different faults in the same faulty phase for better fault tolerance.

B. Two-Mode Minimum-Copper-Loss Fault-Tolerant Control

According to the operation analysis of the faulty inverter leg in Section IV-A, a Phase-X open-switch fault will cause zero Phase-X current in half a fundamental period. The faulty inverter can still work normally in the rest of the fundamental period. Thus, the Phase-X open-switch fault can be considered as the Phase-X open-phase fault during the half fundamental period of abnormal inverter output. The proposed minimum-copper-loss fault-tolerant control for open-phase fault can be directly used to tolerate the open-switch fault during this time. In the other half fundamental period, the remaining healthy switch and diodes in the faulty inverter leg can be fully utilized to further optimize the copper loss in the fault-tolerant operation by giving the current references under normal conditions. In this way, the general copper loss of DT-PMSM under open-switch fault can be reduced greatly. Based on this idea, a two-mode minimum-copper-loss fault-tolerant control is proposed for the open-switch fault of DT-PMSM drives. In Mode-I, the proposed minimum-copper-loss fault-tolerant control for open-phase fault is directly used to tolerate the open-switch fault. In Mode-II, the normal current references are used to further optimize the copper loss.

As analyzed in Section IV-A, the time ranges of normal operation and abnormal operation are determined by the faulty switch and current direction in the faulty inverter leg. Thus, the mode selection in the proposed two-mode minimum-copper-loss fault-tolerant control for open-switch fault is designed according to the faulty switch and current direction in the faulty inverter leg. To improve the precision of transition and simplify the judgment of two fault-tolerant modes, the normal phase current

reference of the faulty phase is utilized to differentiate the positive and negative half fundamental periods. According to (5), the relationships between normal phase current references and electric angle θ_e can be expressed as

$$\begin{cases} i^*_{\mathrm{A-Normal}} = -i^*_q \sin(\theta_e) \\ i^*_{\mathrm{B-Normal}} = -i^*_q \sin(\theta_e - \frac{2\pi}{3}) \\ i^*_{\mathrm{C-Normal}} = -i^*_q \sin(\theta_e + \frac{2\pi}{3}) \\ i^*_{\mathrm{D-Normal}} = -i^*_q \sin(\theta_e - \frac{\pi}{6}) \\ i^*_{\mathrm{E-Normal}} = -i^*_q \sin(\theta_e - \frac{5\pi}{6}) \\ i^*_{\mathrm{F-Normal}} = -i^*_q \sin(\theta_e + \frac{3\pi}{2}). \end{cases} \tag{20}$$

Taking $\mathrm{S_{A1}}$ (upper switch in phase-A) open-switch fault as an example, the direction of normal phase-A current reference can be determined according to (20). The $\mathrm{S_{A1}}$ open-switch fault will cause zero Phase-A current in the positive half fundamental period of $i_{\mathrm{A\text{-}Normal}}$. The faulty inverter can still work normally under $\mathrm{S_{A1}}$ open-switch fault in the negative fundamental period of $i_{\mathrm{A\text{-}Normal}}$. Thus, in the positive half fundamental period of $i_{\mathrm{A\text{-}Normal}}$, the proposed fault-tolerant control for Phase-A open-phase fault is directly used, which is defined as Mode-I. In the negative half fundamental period of $i_{\mathrm{A\text{-}Normal}}$, the normal current references are used to further optimize the copper loss, which is defined as Mode II. Since the fault-tolerant modes under open-switch fault are selected according to the current direction of the faulty phase, not the rotor position, the proposed fault-tolerant control scheme is effective under any mode of four-quadrant operation, including the regenerative mode. For the $\mathrm{S_{A1}}$ open-switch fault of DT-PMSM drives with isolated neutral points, the current references can be obtained in (21) by combining (16) with the rules of mode selection. For the $\mathrm{S_{A1}}$ open-switch fault of DT-PMSM drives with connected neutral points, the current references can be obtained in (22) by combining (19) with the rules of mode selection

$$\begin{cases} i^*_d = \begin{cases} \frac{\sin(2\theta_e)}{3+\cos(2\theta_e)} i^*_q & (i^*_{\mathrm{A-Normal}} > 0) \\ 0 & (i^*_{\mathrm{A-Normal}} < 0) \end{cases} \\ i^*_x = \begin{cases} \frac{2\sin(\theta_e)}{3+\cos(2\theta_e)} i^*_q & (i^*_{\mathrm{A-Normal}} > 0) \\ 0 & (i^*_{\mathrm{A-Normal}} < 0) \end{cases} \\ i^*_y = 0 \\ i^*_{o1} = 0 \\ i^*_{o2} = 0. \end{cases} \tag{21}$$

Based on (21) and (22), the waveforms of the minimum-copper-loss current references on α–β, x–y, and o_1–o_2 subspaces for the open-switch fault of DT-PMSM drive with different winding configurations can be plotted, as shown in Figs. 10(a) and 11(a). It can be observed that the current references in Mode-II of the proposed minimum-copper-loss fault-tolerant control scheme are identical with the current references in normal operation. In this way, the proposed minimum-copper-loss fault-tolerant control scheme for open-switch fault can reduce the copper loss greatly by fully utilizing the remaining healthy switch in the faulty inverter leg. By transforming the current references from the decoupled coordinate system into the six-phase stationary coordinate system, the six-phase current references can be plotted for the configurations of isolated neutral points connected neutral points in Figs. 10(b) and 11(b), respectively.

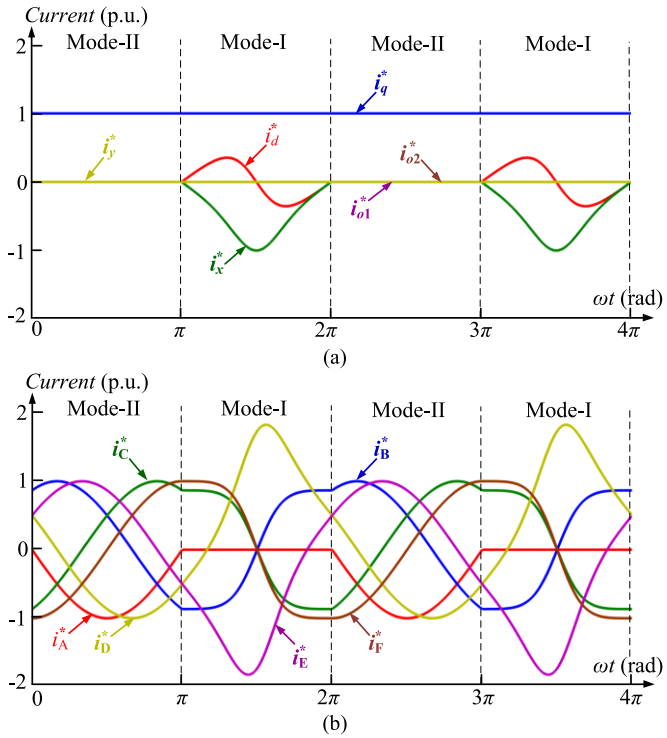

Fig. 10. Current references of the proposed minimum-copper-loss fault-tolerant control for $\mathrm{S_{A1}}$ open-switch fault of DT-PMSM drive with isolated neutral points. (a) Currents on α–β, x–y, and o_1–o_2 subspaces. (b) Phase currents.

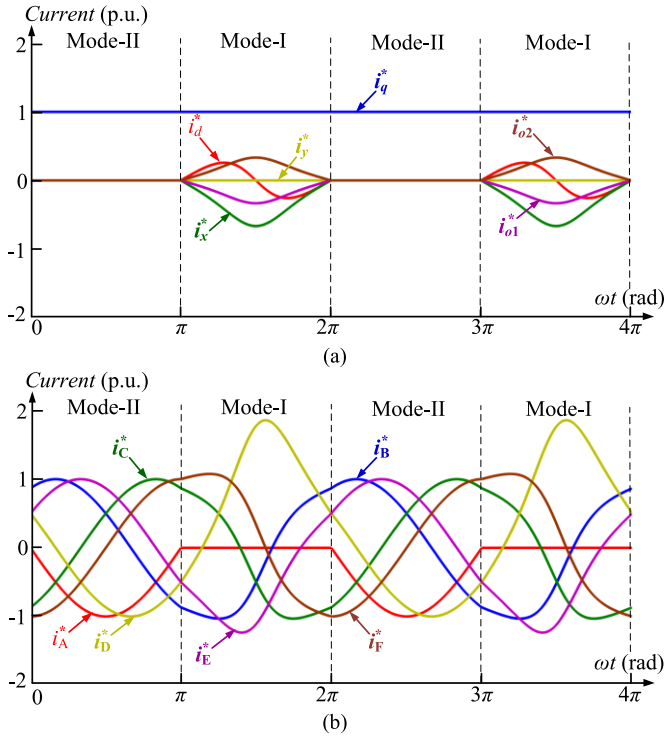

Fig. 11. Current references of the proposed minimum-copper-loss fault-tolerant control for $\mathrm{S_{A1}}$ open-switch fault of DT-PMSM drive with connected neutral points. (a) Currents on α–β, x–y, and o_1–o_2 subspaces. (b) Phase currents.

TABLE I
COMPARISON OF COPPER LOSS

Winding Configuration	Fault-tolerant Schemes	Copper Loss (p.u.)	
		Open phase	Open switch
Isolated neutral points	Minimum-copper-loss scheme I [18]	1.5	1.5
	Minimum-copper-loss scheme II [21]	1.429	1.429
	Proposed minimum-copper-loss scheme	1.414	1.207
Connected neutral points	Minimum-copper-loss scheme III [19]	1.37	1.37
	Proposed minimum-copper-loss scheme	1.291	1.146

It can be proved from Figs. 10 and 11 that the proposed two-mode minimum-copper-loss fault-tolerant control can guarantee smooth transitions between two modes

$$\begin{cases} i_d^* = \begin{cases} \frac{\sin(2\theta_e)}{4+\cos(2\theta_e)} i_q^* & (i^*_{\mathrm{A-Normal}} > 0) \\ 0 & (i^*_{\mathrm{A-Normal}} < 0) \end{cases} \\ i_x^* = \begin{cases} \frac{2\sin(\theta_e)}{4+\cos(2\theta_e)} i_q^* & (i^*_{\mathrm{A-Normal}} > 0) \\ 0 & (i^*_{\mathrm{A-Normal}} < 0) \end{cases} \\ i_y^* = 0 \\ i_{o1}^* = \begin{cases} \frac{\sin(\theta_e)}{4+\cos(2\theta_e)} i_q^* & (i^*_{\mathrm{A-Normal}} > 0) \\ 0 & (i^*_{\mathrm{A-Normal}} < 0) \end{cases} \\ i_{o2}^* = \begin{cases} -\frac{\sin(\theta_e)}{4+\cos(2\theta_e)} i_q^* & (i^*_{\mathrm{A-Normal}} > 0) \\ 0 & (i^*_{\mathrm{A-Normal}} < 0). \end{cases} \end{cases} \tag{22}$$

V. EVALUATION OF COPPER LOSS REDUCTION

To prove the superiority of the proposed minimum-copper-loss fault-tolerant control scheme, it is compared with three existing typical minimum-copper-loss fault-tolerant control schemes, as shown in Table I. The theoretical copper losses of DT-PMSM using different minimum-copper-loss fault-tolerant control schemes are calculated based on (6). For ease of comparison, the copper losses in Table I are expressed in the form of per unit (p.u.). The copper loss under normal operation is considered as 1 p.u. For the open-phase fault of DT-PMSM drive with isolated neutral points, the minimum-copper-loss fault-tolerant control scheme I in [18] can reduce the copper loss to 1.5 p.u. By limiting the d_2-axis current to zero, the minimum-copper-loss scheme II in [21] can further reduce the copper loss to 1.429 p.u., which is known as the lowest copper loss among all minimum-copper-loss schemes for the open-phase fault of DT-PMSM drive with isolated neutral points previously. By removing all unnecessary constraints, the optimal copper loss of 1.414 p.u. is obtained by using the proposed minimum-copper-loss scheme in this article. Thus, an additional 1% copper loss can be saved in this case by using the proposed minimum-copper-loss fault-tolerant control scheme, and the overheating problem in fault-tolerant operation can be relieved accordingly. Conventionally, the inverter leg comprising a faulty switch is usually removed directly, and the fault-tolerant control schemes for open-phase faults can be used to tolerate the open-switch fault. As a result, the same copper losses are generated under open-phase and open-switch faults. Different from these schemes, the proposed minimum-copper-loss fault-tolerant control can reduce the copper loss under open-switch faults from 1.429 p.u. to 1.207 p.u. by fully utilizing the remaining healthy switch in the faulty inverter leg. Thus, an additional 15.5% copper loss can be saved in this case by using the proposed minimum-copper-loss fault-tolerant control scheme.

TABLE II
COMPARISON OF TORQUE OUTPUT CAPABILITY

Winding Configuration	Fault-tolerant Schemes	Maximum RMS current (p.u.)	Torque output capability
Isolated neutral points	Minimum-copper-loss scheme I [18]	1.803	55.5%
	Maximum-torque scheme I [33]	1.732	57.7%
	Minimum-copper-loss scheme II [21]	1.617	61.8%
	Proposed scheme for open-phase fault	1.573	63.6%
	Proposed scheme for open-switch fault	1.318	75.9%
Connected neutral points	Minimum-copper-loss scheme III [19]	1.866	55.4%
	Maximum-torque scheme II [33]	1.441	69.4%
	Proposed scheme for open-phase fault	1.664	60.1%
	Proposed scheme for open-switch fault	1.373	72.8%

For the open-phase fault of DT-PMSM drive with connected neutral points, the proposed minimum-copper-loss fault-tolerant control scheme can reduce the copper loss from the existing lowest value of 1.37 p.u. using the minimum-copper-loss scheme III in [19] to 1.291 p.u. with an additional saving of 5.8% copper loss. Similarly, for the open-switch fault of DT-PMSM drive with connected neutral points, the proposed minimum-copper-loss fault-tolerant control scheme can reduce the copper loss from the existing lowest value of 1.37 p.u. using the minimum-copper-loss scheme III to 1.146 p.u. with an additional saving of 16.4% copper loss. Therefore, the proposed scheme provides an effective solution for copper loss reduction under the fault-tolerant operation of open-switch faults. Based on the aforementioned evaluation of copper loss, the proposed minimum-copper-loss fault-tolerant solution can always save more copper losses than all existing fault-tolerant schemes for both the open-phase fault and the open-switch fault in two-level VSI fed DT-PMSM drives with different winding configurations.

Due to the loss of current contribution from the faulty phase, the rms currents of some phases will become larger than their normal values inevitably to output the same torque. When any phase currents exceed their limits under the fault-tolerant operation, the derating operation should be carried out to avoid the overcurrent problem and secondary faults [10], [33]. Table III compares the torque output capability between the proposed fault-tolerant scheme and the conventional fault-tolerant schemes. The torque output capability, namely the ratio of

TABLE III
KEY PARAMETERS OF EXPERIMENTAL SETUP

Name	*Value*
Pole pair number	3
q-axis inductance	6.21 mH
d-axis inductance	6.21 mH
PM flux (amplitude)	0.2 Wb
Resistance	0.45 Ω
DC link capacitance	1000 uF
Speed reference	500 rpm
Rated phase current	8 A
Rated load	10 Nm
Sampling frequency	5 kHz
Switching frequency	5 kHz

maximum torque in the fault-tolerant operation to the rated torque, can be directly expressed with the derating ratio. Since the phase currents in the proposed scheme are all nonsinusoidal waveforms, the derating ratio of the proposed scheme is calculated with the rms current, not the peak current. In this way, torque output capability can be obtained as the ratio of the rated rms phase current to the maximum rms phase current in the fault-tolerant operation, as shown in Table II. For the case of DT-PMSM drive with isolated neutral points, the torque output capability can be increased from 55.5% in minimum-copper-loss fault-tolerant control scheme I [18] to 57.7% in the maximum-torque scheme I [33] by modifying the optimization constraints. Then, the minimum-copper-loss scheme II in [21] further improves torque output capability to 61.8% by introducing the low-order harmonic components into the current references. By comparison, the proposed scheme possesses the highest torque output capabilities of 63.6% under open-phase fault and 75.9% under open-switch fault. For the case of DT-PMSM drive with connected neutral points, the torque output capability can be greatly improved from 55.4% in minimum-copper-loss fault-tolerant control scheme III [19] to 69.4% in maximum-torque scheme II [33] by modifying the optimization constraints. The torque output capability of the proposed fault-tolerant control scheme is between them under the open-phase fault but achieves a breakthrough of 72.8% under open-switch fault. Since the current references of the proposed fault-tolerant control scheme are derived with the minimum-copper-loss constraints, the proposed fault-tolerant control scheme is not the best solution for maximum torque output. The torque output capability of DT-PMSM drive can be further improved by referring to the ideas of nonsinusoidal current references and the utilization of the remaining healthy switch in the faulty inverter leg from the proposed minimum-copper-loss fault-tolerant control scheme.

It should be noted that the proposed minimum-copper-loss fault-tolerant control scheme focuses on copper loss minimization without specifically considering the switching loss and core loss. For a DT-PMSM drive, the switching loss is mainly determined by switching frequency and conduction current, whereas the core loss is mainly determined by the current frequency and stator flux [34], [35]. Thus, the proposed fault-tolerant control scheme can reduce the general switching losses due to the reductions of the conduction currents, but have no effect on the core loss. The key is that the proposed fault-tolerant control scheme can minimize the copper loss. Finally, the general losses of the DT-PMSM drive will be reduced with the proposed fault-tolerant control scheme but not be minimized. Further reduction of switching loss and core loss under open-switch fault and open-phase fault of DT-PMSM drive can be achieved by combining the proposed fault-tolerant control scheme with some other loss reduction techniques [36]–[38].

VI. EXPERIMENTAL VERIFICATION

The experiments are carried out on a laboratory prototype of two-level VSI fed DT-PMSM drive to verify the effectiveness of the proposed minimum-copper-loss fault-tolerant control scheme. In the experiment, the DSP (TMS320F28335) is adopted to perform the control algorithm and generate the PWM signals. A permanent-magnetic generator is coupled to the three-phase PMSM to provide the electric load. The load torque can be changed by adjusting the resistance box. The open-phase fault is performed by disconnecting the breaker of the faulty phase. The open-switch fault is constructed by forcing the driving signal of the corresponding IGBT device to be low all along. The key parameters of the experimental platform are shown in Table III. In this article, two experimental methods have been adopted to prove the effectiveness of the proposed minimum-copper-loss fault-tolerant control scheme. The derived current references under different cases have been proved to generate the corresponding lowest copper losses. If the real-time currents can track their time-vary current references with the designed uniform control diagram in the experiment, the minimized copper losses can be proved. Thus, both the current references and the current feedbacks on α–β, x–y, and o_1–o_2 subspaces have been presented in Fig. 12–Fig. 16 to prove the effectiveness of the proposed scheme. The second experimental method adopted in this article is evaluating the matching degrees between theoretical minimum copper losses in Table I and experimental copper losses under different cases. In the experiment, the average copper losses of the proposed minimum-copper-loss fault-tolerant control scheme under different cases are calculated according to (6).

Fig. 12 shows the proposed minimum-copper-loss fault-tolerant control for Phase-A open-phase fault of DT-PMSM drive with isolated neutral points under 500-r/min speed and 10-N·m load. It can be observed from Fig. 12(a) to (c) that the current references on α–β, x–y, and o_1–o_2 subspaces match well with the current waveforms in Fig. 4(a). The currents on α–β, x–y, and o_1–o_2 subspaces can all track their corresponding current references precisely, as shown in Fig. 12(a)–(c). Since the scope adopted in the experiment (Tektronix TPS2014B) only has four channels, the Phase-ABC currents and Phase-DEF currents are presented in two separate windows, as shown in Fig. 12(d) and (e). Owing to the precise closed-loop current control, the experimental phase currents match well with the corresponding theoretical waveforms in Fig. 4(b). In the fault-tolerant operation, the fluctuating torque outputs of two three-phase windings, namely T_{e1} and T_{e2}, can merge with each other to generate stable general torque output and speed, as shown in Fig. 12(f).

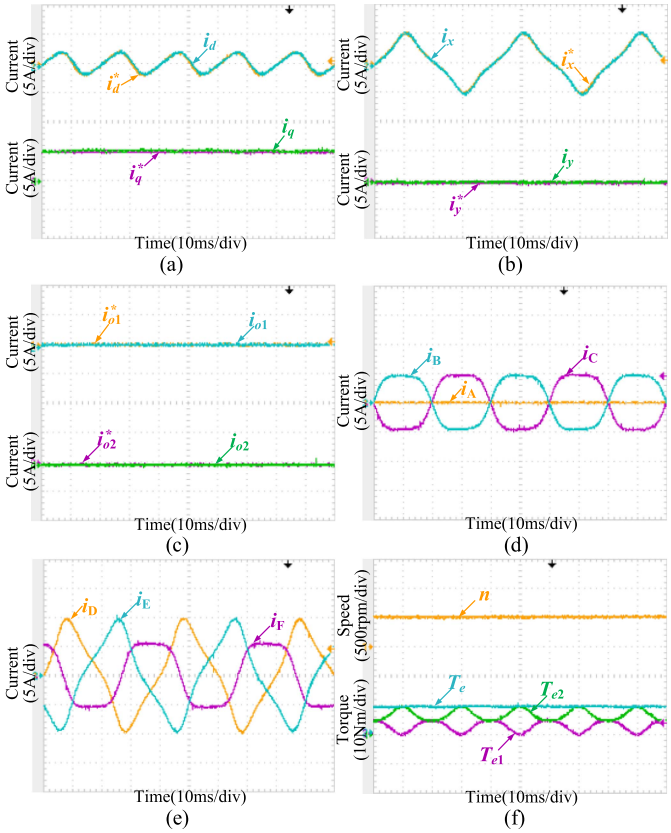

Fig. 12. Measured results of proposed fault-tolerant control for Phase-A open-phase fault of DT-PMSM drive with isolated neutral points. (a) d-axis and q-axis currents. (b) x-axis and y-axis currents. (c) o_1-axis and o_2-axis currents. (d) Phase-ABC currents. (e) Phase-DEF currents. (f) Speed and torque.

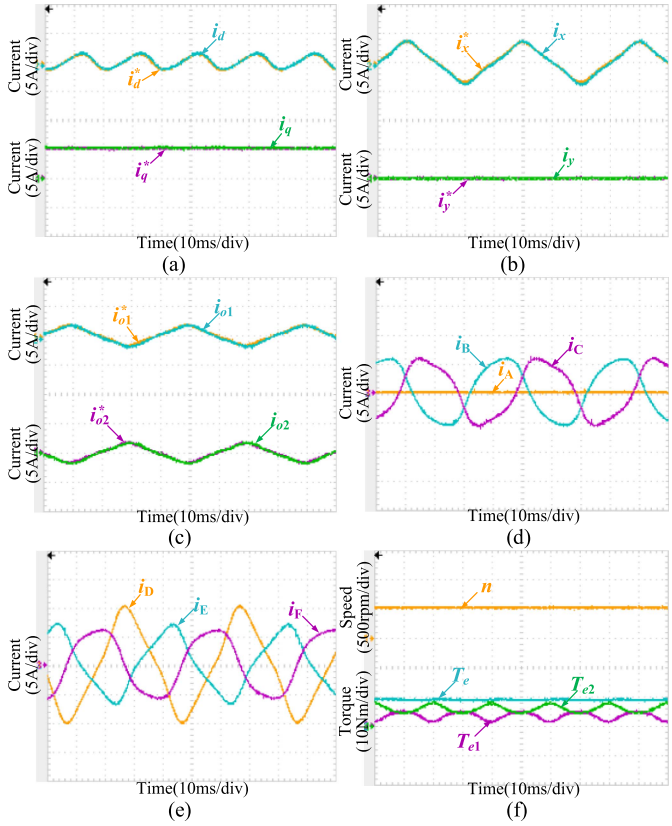

Fig. 13. Measured results of proposed fault-tolerant control for Phase-A open-phase fault of DT-PMSM drive with connected neutral points. (a) d-axis and q-axis currents. (b) x-axis and y-axis currents. (c) o_1-axis and o_2-axis currents. (d) Phase-ABC currents. (e) Phase-DEF currents. (f) Speed and torque.

The experimental results in Fig. 12 verify the effectiveness of the proposed fault-tolerant control for the open-phase fault of DT-PMSM drive with isolated neutral points.

Fig. 13 presents the proposed fault-tolerant control for Phase-A open-phase fault of DT-PMSM drive with connected neutral points under 500-r/min speed and 10-N·m load. It can be observed from Fig. 13(a) to (c) that the current references on α–β, x–y, and o_1–o_2 subspaces match well with the current waveforms in Fig. 5(a). The currents on α–β, x–y, and o_1–o_2 subspaces can all track their corresponding current references precisely, as shown in Fig. 13(a)–(c). Compared with the x-axis current references in Fig. 12(b), the x-axis current references in Fig. 13(b) can be reduced obviously by using the zero-sequence current path. In this way, the general copper loss can be further reduced. Owing to the precise closed-loop current control, the measured phase currents in Fig. 13(d) and (e) match well with the corresponding theoretical waveforms in Fig. 5(b). In the fault-tolerant operation, the fluctuating torque outputs of two three-phase windings, namely T_{e1} and T_{e2}, can merge with each other to generate stable general torque output and speed, as shown in Fig. 13(f). The experimental results in Fig. 13 verify the effectiveness of the proposed fault-tolerant control for the open-phase fault of DT-PMSM drive with connected neutral points.

Figs. 14 and 15 show the proposed minimum-copper-loss fault-tolerant control for S_{A1} open-switch fault of DT-PMSM drive with isolated neutral points and connected neutral points under 500-r/min speed and 10-N·m load, respectively. It can be observed from Fig. 14(a) to (c) and Fig. 15(a) to (c) that the current references on α–β, x–y, and o_1–o_2 subspaces match well with the current waveforms in Figs. 10(a) and 11(a), respectively. The currents on α–β, x–y, and o_1–o_2 subspaces can all track their corresponding current references precisely. It can be observed that the currents in Mode-II of the proposed minimum-copper-loss fault-tolerant control scheme are identical with the corresponding currents in normal operation. In this way, the proposed minimum-copper-loss fault-tolerant control scheme for open-switch fault can reduce the copper loss greatly by fully utilizing the remaining healthy switch in the faulty inverter leg. Owing to the precise closed-loop current control, the measured phase currents in Figs. 14 and 15 match well with the corresponding theoretical waveforms in Figs. 10(b) and 11(b), respectively. In the fault-tolerant operation, the fluctuating torque outputs of two three-phase windings, namely T_{e1} and T_{e2}, can merge with each other to generate the stable torque and speed, as shown in Figs. 14(f) and 15(f).

Fig. 16 shows the copper losses of different fault cases of DT-PMSM drive with different winding configurations from the normal operation to the fault-tolerant operation. In the experiment, the copper losses are calculated by substituting the real-time phase currents into (6). To distinguish different fault cases, two representative phase currents, namely Phase-A current i_A and Phase-E current i_E, are presented together with the

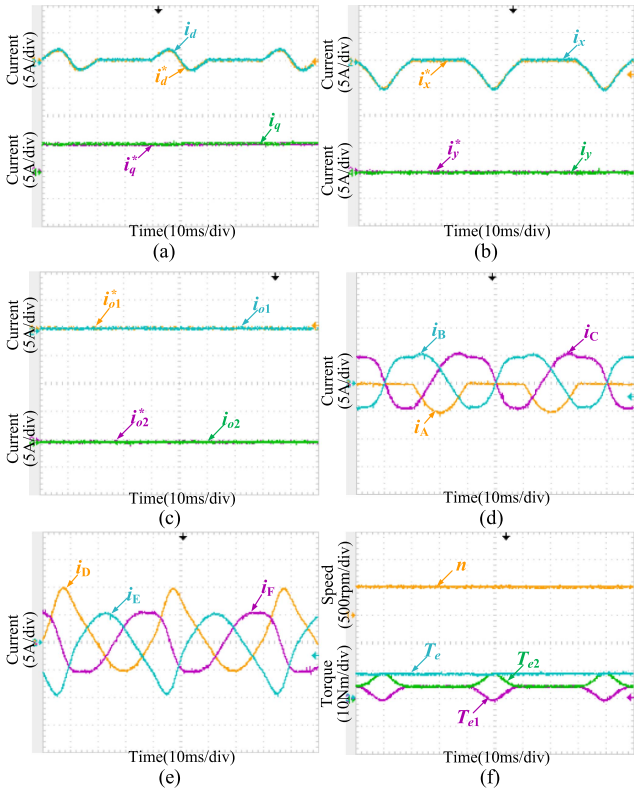

Fig. 14. Measured results of proposed fault-tolerant control for S_{A1} open-switch fault of DT-PMSM drive with isolated neutral points. (a) d-axis and q-axis currents. (b) x-axis and y-axis currents. (c) o_1-axis and o_2-axis currents. (d) Phase-ABC currents. (e) Phase-DEF currents. (f) Speed and torque.

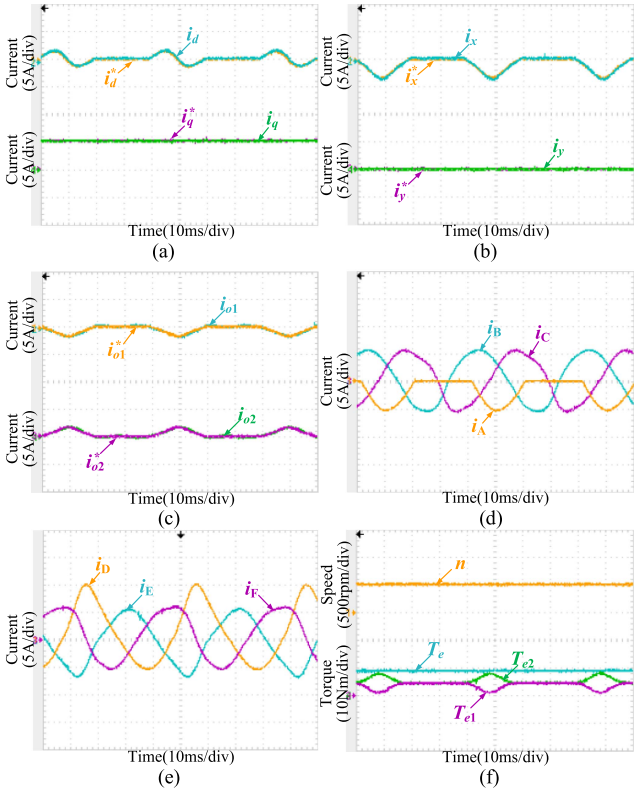

Fig. 15. Measured results of proposed fault-tolerant control for S_{A1} open-switch fault of DT-PMSM drive with connected neutral points. (a) d-axis and q-axis currents. (b) x-axis and y-axis currents. (c) o_1-axis and o_2-axis currents. (d) Phase-ABC currents. (e) Phase-DEF currents. (f) Speed and torque.

copper loss waveform. In the case of Phase-A open-phase fault of DT-PMSM drive with isolated neutral points, the Phase-A current is forced to be zero instantly and the amplitude of Phase-E current increases obviously, as shown in Fig. 16(a). Meanwhile, the copper loss increases from 36.4 W in normal operation to 51.4 W in fault-tolerant operation. In the case of Phase-A open-phase fault of DT-PMSM drive with connected neutral points, the Phase-A current is forced to be zero after fault and the amplitude of Phase-E current increases slightly, as shown in Fig. 16(b). Meanwhile, the copper loss increases from 36.4 W in normal operation to 47.5 W in fault-tolerant operation. In the cases of S_{A1} open-switch fault of DT-PMSM drive with isolated and connected neutral points, the positive half parts of Phase-A currents are forced to be zeros after fault and the negative parts of Phase-A currents remain normal, as shown in Fig. 16(c) and (d). Besides, only the negative parts of the Phase-E currents in Fig. 16(c) and (d) are changed after fault. The copper losses increase from 36.4 W in normal operation to 44.1 and 45.6 W in fault-tolerant operation. It can be observed from Fig. 16 that the per-unit copper losses of the proposed fault-tolerant control for different fault cases are 1.412, 1.305, 1.212, and 1.151, respectively. These results are highly close to the corresponding theoretical values of 1.414, 1.291, 1.207, and 1.146 in Table I. Thus, the effective copper loss reductions of the proposed fault-tolerant control for different fault cases of the open-phase fault and open-switch fault of DT-PMSM drive with different winding configurations can be proved.

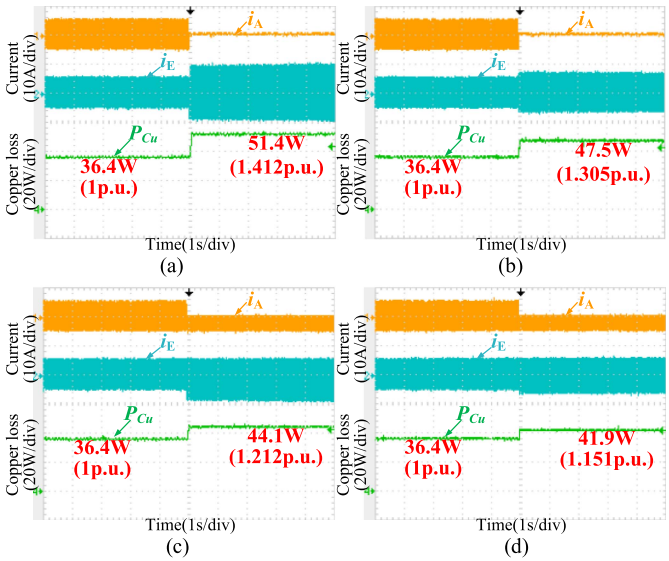

Fig. 16. Measured copper losses of the proposed fault-tolerant control for different fault cases of DT-PMSM drive with different winding configurations. (a) Phase-A open-phase fault and isolated neutral points. (b) Phase-A open-switch fault and connected neutral points. (c) S_{A1} open-switch fault and isolated neutral points. (d) S_{A1} open-switch fault and connected neutral points.

To prove the effectiveness of the proposed fault-tolerant control scheme during the dynamic process, the simulation results with speed response and torque response are presented in

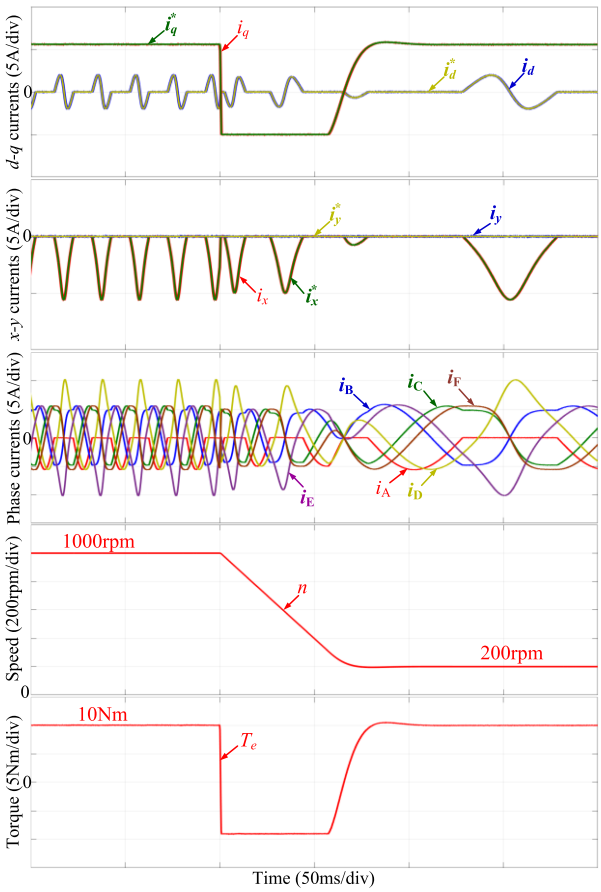

Fig. 17. Speed response of the proposed fault-tolerant control for S_{A1} open-switch fault in DT-PMSM drive with isolated neutral points via simulation.

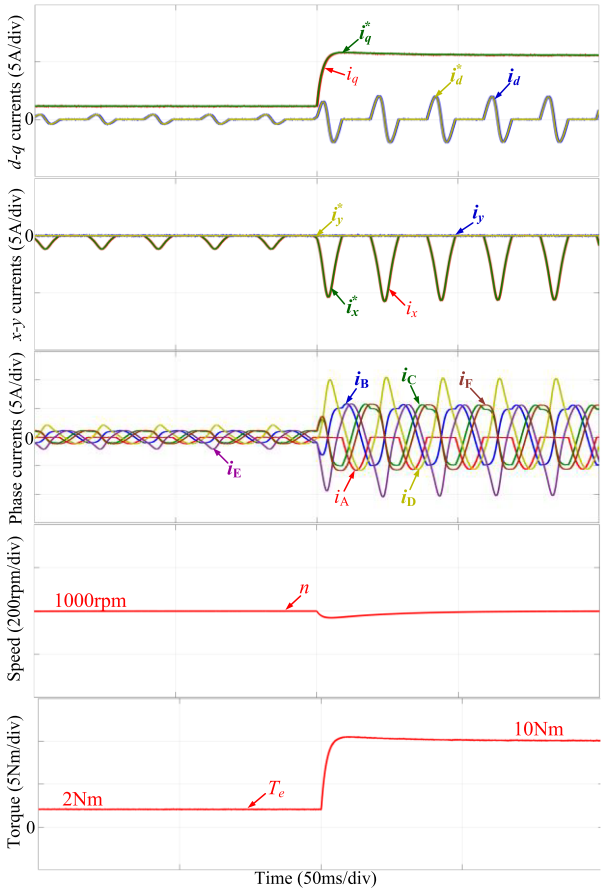

Fig. 18. Torque response of the proposed fault-tolerant control for S_{A1} open-switch fault in DT-PMSM drive with isolated neutral points via simulation.

Figs. 17 and 18. Fig. 17 shows the speed response of the proposed fault-tolerant control for S_{A1} open-switch fault in DT-PMSM drive with isolated neutral points. In Fig. 17, the speed reference is suddenly changed from 1000 to 200-r/min under 10-N·m load. It can be found that the currents on α–β and x–y subspaces can all track their corresponding current references precisely even under the regenerative state. The six-phase currents operate as expected. During the transition, the currents and torques respond quickly to the speed change. Due to the adoption of the current limitation for the q-axis current, the q-axis current i_q and the electromagnetic torque T_e both reach stable values quickly under the regenerative state. Finally, the rotor speed n reaches it references of 200 r/min in 100 ms. Fig. 17 proves that the proposed fault-tolerant control scheme is effective in any mode of four-quadrant operation and can achieve fast and precise speed response. Fig. 18 shows the torque response of the proposed fault-tolerant control for S_{A1} open-switch fault in DT-PMSM drive with isolated neutral points. In Fig. 18, the load torque is suddenly increased from 2 to 10 N·m under 1000-r/min speed. During the whole process of torque response, the currents on α–β and x–y subspaces can all track their corresponding current references precisely and the six-phase currents operate as expected. During the transition, the speed slightly drops and return to normal quickly with a stable torque output of 10 N·m. Fig. 18 proves that the effectiveness of the proposed fault-tolerant control scheme under speed response.

VII. Conclusion

This article proposed a minimum-copper-loss fault-tolerant control scheme for open-phase fault and open-switch fault of DT-PMSM drives. Both the winding configurations of isolated neutral points and connected neutral points are considered in this article. In the proposed fault-tolerant control scheme, the current references with the theoretical lowest copper losses are first derived and applied for open-phase fault and open-switch fault of DT-PMSM drives. Besides, in the proposed fault-tolerant control scheme for the open-switch fault of DT-PMSM drives, the copper losses are further reduced by fully utilizing the remaining healthy switch in the faulty inverter leg. Theoretically, the proposed fault-tolerant control scheme can save at least 1%, 5.8%, 15.5%, and 16.4% copper losses than existing fault-tolerant control schemes for corresponding open-phase faults and open-switch faults of the typical two-level VSI fed DT-PMSM drives with isolated neutral points and connected neutral points. The effectiveness of the proposed fault-tolerant control scheme has been verified by experiments.

References

[1] E. Levi, F. Barrero, and M. J. Duran, "Multiphase machines and drives—Revisited," *IEEE Trans. Ind. Electron.*, vol. 63, no. 1, pp. 429–432, Jan. 2016.

[2] J. W. Bennett, B. C. Mecrow, D. J. Atkinson, and G. J. Atkinson, "Safety-critical design of electromechanical actuation systems in commercial aircraft," *IET Elect. Power Appl.*, vol. 5, no. 1, pp. 37–47, Jan. 2011.
[3] Z. Liu, J. Wu, and L. Hao, "Coordinated and fault-tolerant control of tandem 15-phase induction motors in ship propulsion system," *IET Elect. Power Appl.*, vol. 12, no. 1, pp. 91–97, Jan. 2018.
[4] Z. Wang, X. Wang, X. Yang, C. Wen, Y. Gong, and Y. Hu, "Mitigation of DC-link current ripple for dual three-phase flux-adjustable hybrid PMAC drives using collaborative switching strategy," *IEEE Trans. Ind. Electron.*, vol. 67, no. 9, pp. 7202–7216, Sep. 2020.
[5] E. Levi, R. Bojoi, F. Profumo, H. A. Toliyat, and S. Williamson, "Multiphase induction motor drives—A technology status review," *IET Elect. Power Appl.*, vol. 1, no. 4, pp. 489–516, Jul. 2007.
[6] L. Zhang, Y. Fan, R. Cui, R. D. Lorenz, and M. Cheng, "Fault-tolerant direct torque control of five-phase FTFSCW-IPM motor based on analogous three-phase SVPWM for electric vehicle applications," *IEEE Trans. Veh. Technol.*, vol. 67, no. 2, pp. 910–919, Feb. 2018.
[7] M. Priestley, M. Farshadnia, and J. E. Fletcher, "FOC transformation for single open-phase faults in the five-phase open-end winding topology," *IEEE Trans. Ind. Electron.*, vol. 67, no. 2, pp. 842–851, Feb. 2020.
[8] X. Wang, Z. Wang, M. Gu, D. Xiao, J. He, and A. Emadi, "Diagnosis-free self-healing scheme for open-circuit faults in dual three-phase PMSM drives," *IEEE Trans. Power Electron.*, vol. 35, no. 11, pp. 12053–12071, Nov. 2020.
[9] J. Kong, K. Wang, J. Zhang, and H. Zhang, "Multiple open-switch fault diagnosis for five-phase permanent magnet machine utilizing currents in stationary reference frame," *IEEE Trans. Energy Convers.*, vol. 36, no. 1, pp. 314–324, Mar. 2021.
[10] E. Levi, "Multiphase electric machines for variable-speed applications," *IEEE Trans. Ind. Electron.*, vol. 55, no. 5, pp. 1893–1909, May 2008.
[11] X. Jiang, W. Huang, R. Cao, Z. Hao, and W. Jiang, "Electric drive system of dual-winding fault tolerant permanent-magnet motor for aerospace applications," *IEEE Trans. Ind. Electron.*, vol. 62, no. 12, pp. 7322–7330, Dec. 2015.
[12] M. Bermudez, I. Gonzalez-Prieto, F. Barrero, H. Guzman, M. J. Duran, and X. Kestelyn, "Open-phase fault-tolerant direct torque control technique for five-phase induction motor drives," *IEEE Trans. Ind. Electron.*, vol. 64, no. 2, pp. 902–911, Feb. 2017.
[13] W. Huang, W. Hua, F. Chen, M. Hu, and J. Zhu, "Model predictive torque control with SVM for five-phase PMSM under open-circuit fault condition," *IEEE Trans. Power Electron.*, vol. 35, no. 5, pp. 5531–5540, May 2020.
[14] B. Tian, Q. An, J. Duan, D. Sun, L. Sun, and D. Semenov, "Decoupled modeling and nonlinear speed control for five-phase PM motor under single-phase open fault," *IEEE Trans. Power Electron.*, vol. 32, no. 7, pp. 5473–5486, Jul. 2017.
[15] Q. Chen, W. Zhao, G. Liu, and Z. Lin, "Extension of virtual-signal-injection-based MTPA control for five-phase IPMSM into fault-tolerant operation," *IEEE Trans. Ind. Electron.*, vol. 66, no. 2, pp. 944–955, Feb. 2019.
[16] H. Lu, J. Li, R. Qu, D. Ye, and Y. Lu, "Fault-tolerant predictive control of six-phase PMSM drives based on pulsewidth modulation," *IEEE Trans. Ind. Electron.*, vol. 66, no. 7, pp. 4992–5003, Jul. 2019.
[17] G. Feng, C. Lai, W. Li, J. Tjong, and N. C. Kar, "Open-Phase fault modeling and optimized fault-tolerant control of dual three-phase permanent magnet synchronous machines," *IEEE Trans. Power Electron.*, vol. 34, no. 11, pp. 11116–11127, Nov. 2019.
[18] I. González-Prieto, M. J. Duran, and F. J. Barrero, "Fault-tolerant control of six-phase induction motor drives with variable current injection," *IEEE Trans. Power Electron.*, vol. 32, no. 10, pp. 7894–7903, Oct. 2017.
[19] H. S. Che, M. J. Duran, E. Levi, M. Jones, W. Hew, and N. A. Rahim, "Postfault operation of an asymmetrical six-phase induction machine with single and two isolated neutral points," *IEEE Trans. Power Electron.*, vol. 29, no. 10, pp. 5406–5416, Oct. 2014.
[20] M. Shamsi-Nejad, B. Nahid-Mobarakeh, S. Pierfederici, and F. Meibody-Tabar, "Fault tolerant and minimum loss control of double-star synchronous machines under open phase conditions," *IEEE Trans. Ind. Electron.*, vol. 55, no. 5, pp. 1956–1965, May 2008.
[21] W. Wang, J. Zhang, M. Cheng, and S. Li, "Fault-tolerant control of dual three-phase permanent-magnet synchronous machine drives under open-phase faults," *IEEE Trans. Power Electron.*, vol. 32, no. 3, pp. 2052–2063, Mar. 2017.
[22] X. Wang, Z. Wang, M. Gu, D. Xiao, J. He, and A. Emadi, "Diagnosis-free self-healing scheme for open-circuit faults in dual three-phase PMSM drives," *IEEE Trans. Power Electron.*, vol. 35, no. 11, pp. 12053–12071, Nov. 2020.
[23] M. Tousizadeh, H. S. Che, J. Selvaraj, N. A. Rahim, and B. Ooi, "Performance comparison of fault-tolerant three-phase induction motor drives considering current and voltage limits," *IEEE Trans. Ind. Electron.*, vol. 66, no. 4, pp. 2639–2648, Apr. 2019.
[24] X. Zhou, J. Sun, H. Li, M. Lu, and F. Zeng, "PMSM open-phase fault-tolerant control strategy based on four-leg inverter," *IEEE Trans. Power Electron.*, vol. 35, no. 3, pp. 2799–2808, Mar. 2020.
[25] B. Mirafzal, "Survey of fault-tolerance techniques for three-phase voltage source inverters," *IEEE Trans. Ind. Electron.*, vol. 61, no. 10, pp. 5192–5202, Oct. 2014.
[26] X. Wang, Z. Wang, M. Cheng, and Y. Hu, "Remedial strategies of T-NPC three-level asymmetric six-phase PMSM drives based on SVM-DTC," *IEEE Trans. Ind. Electron.*, vol. 64, no. 9, pp. 6841–6853, Sep. 2017.
[27] X. Wang, Z. Wang, Z. Xu, J. He, and W. Zhao, "Diagnosis and tolerance of common electrical faults in T-type three-level inverters fed dual three-phase PMSM drives," *IEEE Trans. Power Electron.*, vol. 35, no. 2, pp. 1753–1769, Feb. 2020.
[28] J. D. Dasika and M. Saeedifard, "A fault-tolerant strategy to control the matrix converter under an open-switch failure," *IEEE Trans. Ind. Electron.*, vol. 62, no. 2, pp. 680–691, Feb. 2015.
[29] Y. Zhang, T. Zhao, H. Jing, J. Li, and X. Gui, "A robust deadbeat predictive control scheme for dual three-phase PMSM," in *Proc. Int. Conf. Elect. Mach. System*, 2018, pp. 1223–1228.
[30] L. Malesani, P. Mattavelli, and S. Buso, "Robust dead-beat current control for PWM rectifiers and active filters," *IEEE Trans. Ind. Appl.*, vol. 35, no. 3, pp. 613–620, May/Jun. 1999.
[31] T. Tao, W. Zhao, Y. He, Y. Cheng, S. Saeed, and J. Zhu, "Enhanced fault-tolerant model predictive current control for a five-phase PM motor with continued modulation," *IEEE Trans. Power Electron.*, vol. 36, no. 3, pp. 3236–3246, Mar. 2021.
[32] X. Wang, Z. Wang, Z. Xu, M. Cheng, W. Wang, and Y. Hu, "Comprehensive diagnosis and tolerance strategies for electrical faults and sensor faults in dual three-phase PMSM drives," *IEEE Trans. Power Electron.*, vol. 34, no. 7, pp. 6669–6684, Jul. 2019.
[33] W. N. W. A. Munim, M. J. Duran, H. S. Che, M. Bermúdez, I. González-Prieto, and N. A. Rahim, "A unified analysis of the fault tolerance capability in six-phase induction motor drives," *IEEE Trans. Power Electron.*, vol. 32, no. 10, pp. 7824–7836, Oct. 2017.
[34] F. L. Mapelli, D. Tarsitano, and M. Mauri, "Plug-in hybrid electric vehicle: Modeling, prototype realization, and inverter losses reduction analysis," *IEEE Trans. Ind. Electron.*, vol. 57, no. 2, pp. 598–607, Feb. 2010.
[35] N. Urasaki, T. Senjyu, and K. Uezato, "A novel calculation method for iron loss resistance suitable in modeling permanent-magnet synchronous motors," *IEEE Trans. Energy Convers.*, vol. 18, no. 1, pp. 41–47, Mar. 2003.
[36] C. Xu and S. Lu, "Practical online modulation method for current ripple and switching losses reduction in the three-phase voltage source inverters," *IEEE Trans. Power Electron.*, vol. 36, no. 2, pp. 1475–1490, Feb. 2021.
[37] J. Hang, H. Wu, S. Ding, Y. Huang, and W. Hua, "Improved loss minimization control for IPMSM using equivalent conversion method," *IEEE Trans. Power Electron.*, vol. 36, no. 2, pp. 1931–1940, Feb. 2021.
[38] J. Zheng, W. Zhao, and J. Ji, "Sleeve design of permanent-magnet machine for low rotor losses," *Chin. J. Elect. Eng.*, vol. 6, no. 4, pp. 86–96, Dec. 2020.

Xueqing Wang (Member, IEEE) received the B.S. degree from the Tianjin University of Science and Technology, Tianjin, China, in 2014, and the M.S. and Ph.D. degrees from Southeast University, Nanjing, China, in 2016 and 2020, respectively, all in electrical engineering.

From 2018 to 2019, he was a Joint Ph.D. Student with McMaster Automotive Resource Centre, McMaster University, Hamilton, ON, Canada. He is currently an Associate Research Fellow with the College of Electrical Engineering, Sichuan University, Chengdu, China. His research interests include fault diagnosis and tolerant control of motor drive, multilevel PWM strategy, and control of multiphase permanent magnet synchronous motor.

Zheng Wang (Senior Member, IEEE) received the B.Eng. and M.Eng. degrees from Southeast University, Nanjing, China, in 2000 and 2003, respectively, and the Ph.D. degree from The University of Hong Kong, Hong Kong, in 2008, all in electrical engineering.

From 2008 to 2009, he was a Postdoctoral Fellow with Ryerson University, Toronto, ON, Canada. He is currently a Full Professor with the School of Electrical Engineering, Southeast University. He has authored or coauthored more than 80 internationally refereed papers and four books in his research interests, which include electric drives, power electronics, and distributed generation.

Prof. Wang was the recipient of several academic awards including the IEEE PES Chapter Outstanding Engineer Award, the Best Paper Award of International Conference on Electrical Machines and Systems (ICMES), the Best Session Paper Award of IEEE Annual Meeting of Industrial Electronics (IECON), and the Nanjing Outstanding Paper Award of Natural Science.

Mingzhi He (Member, IEEE) received the B.S. and M.S. degrees from the College of Electrical Engineering, Sichuan University, Chengdu, China, in 2002 and 2004, respectively, and the Ph.D. degree from Southwest Jiaotong University, Chengdu, in 2008.

He is currently a Professor with the College of Electrical Engineering, Sichuan University. His research interests include the control and topology of switching power supply, photovoltaic system, battery charger, and protection.

Qun Zhou (Member, IEEE) received the M.S. and Ph.D. degrees in automation engineering from the University of Electronic Science and Technology of China, Chengdu, China, in 1989 and 2009, respectively.

She is currently a Professor with the College of Electrical Engineering, Sichuan University. Her research interests include power quality analysis and control.

Xueshan Liu (Member, IEEE) received the B.S. degree in communication engineering and the M.S. and Ph.D. degrees in electrical engineering from Southwest Jiaotong University, Chengdu, China, in 2005, 2010, and 2016, respectively.

From 2005 to 2008, he was a Development Engineer for switching-mode power supplies in Asia Power Devices, Inc., Shenzhen, China. From 2010 to 2016, he was a Senior Application Engineer in O2Micro International, Ltd., Chengdu, China. He is currently an Associate Professor with the College of Electrical Engineering, Sichuan University. His research interests include control technique of switching-mode power supply, power factor correction converter and the application of power electronic systems.

Xin Meng (Member, IEEE) received the B.S. degree from the University of Electronic Science and Technology of China, Chengdu, China, in 2014, and the Ph.D. degree from Xi'an Jiaotong University, Xi'an, China, in 20199, both in in electrical engineering.

He was a Faculty Member with Electrical Engineering School, Sichuan University. His research interests include the control of parallel three-phase inverters for uninterrupted power-supply and microgrid application, such as VSG control, droop control, and seamless transfer between grid-connected mode and islanding mode.